mathematics

MDPI

Article

Searching for a Unique Exciton Model of Photosynthetic Pigment–Protein Complexes: Photosystem II Reaction Center Study by Differential Evolution

Denis D. Chesalin and Roman Y. Pishchalnikov *

Prokhorov General Physics Institute of the Russian Academy of Sciences, 119991 Moscow, Russia; genoa-and-pittsburgh@mail.ru
* Correspondence: rpishchal@kapella.gpi.ru; Tel.:+7-499-503-8777

Abstract: Studying the optical properties of photosynthetic pigment–protein complexes (PPCs) in the visible light range, both experimentally and theoretically, is one of the ways of gaining knowledge about the function of the photosynthetic machinery of living species. To simulate the PPC optical response, it is necessary to use semiclassical theories describing the effect of external fields–matter interaction, energy migration in molecular crystals, and electron–phonon coupling. In this paper, we report the results of photosystem II reaction center (PSIIRC) linear optical response simulations. Applying the multimode Brownian oscillator model and the theory of molecular excitons, we have demonstrated that the absorption, circular and linear dichroism, and steady-state fluorescence of PSIIRC can be accurately fitted with the help of differential evolution (DE), the multiparametric evolutionary optimization algorithm. To explore the effectiveness of DE, we used the simulated experimental data as the target functions instead of those actually measured. Only 2 of 10 DE strategies have shown the best performance of the optimization algorithm. With the best tuning parameters of DE/rand-to-best/1/exp strategy determined from the strategy tests, we found the exact solution for the PSIIRC exciton model and fitted the spectra with a reasonable convergence rate.

Keywords: differential evolution; evolutionary computations; chlorophyll; absorption; cumulant expansion; multimode Brownian oscillator model; inhomogeneous broadening; photosystem II reaction center

Citation: Chesalin, D.D.; Pishchalnikov, R.Y. Searching for a Unique Exciton Model of Photosynthetic Pigment–Protein Complexes: Photosystem II Reaction Center Study by Differential Evolution. *Mathematics* **2022**, *10*, 959. https://doi.org/10.3390/math10060959

Academic Editors: Antonin Ponsich, Mariona Vila Bonilla and Bruno Domenech

Received: 22 February 2022
Accepted: 15 March 2022
Published: 17 March 2022

1. Introduction

Among the numerous proteins of living organisms, pigment–protein complexes (PPCs) are perhaps the most interesting object for numerical simulations of the optical response of proteins [1,2] simply because they control the light-driven reactions of the photosynthetic process in organisms that transform light energy into chemical energy. With chlorophylls, bacteriochlorophylls, and carotenoids as the main pigment molecules, PPCs actively absorb from 300 to 900 nm, providing effective light harvesting in the visible range and subsequent energy transport within a complex and between different complexes [3]. The optical properties of individual pigments usually determine those of the whole PPC; however, in some cases, the interaction energies between pigments in PPC and the local binding proteins have much greater effect on the PPC's optical response [1]. The number of pigments in PPCs is crucial as well; it varies from a single carotenoid, such as in the orange carotenoid protein (OCP) complex [4]; dozens of chlorophylls, such as in the trimeric Fenna–Matthews–Olson complex [5–7]; hundreds of chlorophylls, such as in photosystem I [8,9]; and thousands of bacteriochlorophylls, such as in chlorosomes [10].

The main feature of the electronic absorption bands of photosynthetic pigments is a phonon wing, the shape and intensity of which depends on the electron–phonon interaction [11]. Chlorophylls and bacteriochlorophylls are characterized by a set of several dozen vibronic states and a relatively weak electron–phonon interaction, while carotenoids

have four pronounced vibronic states and strongly interact with the electronic states of a pigment [12]. All of these features can be taken into account within the framework of a theory called the multimode Brownian oscillator model (MBOM) [13]. This theory allows for simulating a realistic absorption lineshape of an electronic transition of any pigment by introducing the spectral density function [14]. The shape of a pigment absorption spectrum is modeled by considering that an electronic transition is coupled to a set of effective vibronic modes. Each mode is described by three parameters: the frequency, the damping factor, and the Huang–Rhys factor (otherwise the electron–phonon coupling) [15]. The first two parameters can be estimated experimentally, while the only way to obtain the Huang–Rhys factor is by modeling the pigment's optical response. Thus, by combining the results of experimental analysis and theoretical modeling, we can determine a characteristic set of microparameters for a pigment molecule and use them in further modeling.

In order to model the linear optical properties in the case of an assembly of interacting pigment molecules, it is necessary to use the theory of molecular excitons [16] in addition to MBOM. According to this theory, any system of interacting molecules of an arbitrary geometry and dimensionally is described by the Frenkel exciton Hamiltonian, which is the basis for the theory of molecular crystals [17]. Thus, combining the MBOM and the exciton theory, the system's optical response can be simulated with a high degree of accuracy. There are many studies in which the combination of these two theories was used to obtain realistic simulated spectra and kinetics of various PPCs. Nevertheless, the main disadvantage of these works is the lack of optimization of the experimental data fitting procedure; evidence of the uniqueness of the theoretical models are usually not given.

The use of evolution optimization algorithms [18,19], in particular differential evolution (DE) [20,21], has shown that the search for optimal quantum models of primary photosynthesis processes is possible [22,23]. As opposed to genetic evolutionary algorithms, DE creates a new generation of model parameters, perturbing the current generation with the scaled difference of randomly selected population members. The detailed introduction to DE can be found in different surveys of the topic [24,25]; including descriptions of some modifications of the classical version of the algorithm designed to improve the convergence of DE [26–29].

The aim of our study is to explore, for the first time, the potential of DE to be an effective optimization routine for the fitting of the PPC optical response. We have chosen the reaction center of photosystem II (PSIIRC) as an example of PPCs (Figure 1), the linear spectra of which should be simulated and an appropriate exciton model created [30–33]. PSIIRC is a rather small protein. It contains only eight cofactors embedded in the protein matrix: six chlorophylls (Chl) and two pheophytins [34]. The eight pigments in PSIIRC give us an optically active, eight-level excitonic manifold; however, PSIIRC also has three so-called charge separation states [31], which are optically inactive and will not be considered in our simulations. For the sake of simplicity and clarity, we will use the pre-calculated linear spectra of PSIIRC as target functions instead of the actually measured ones. The absence of noise in the spectra will allow us to estimate the DE convergence with great accuracy.

The statement of the optimization problem is considered in the second section. The DE algorithm and the references that describe its applications for the modeling of the optical response of photosynthetic pigments are discussed in the third section. In the fourth section, we briefly survey some important aspects of quantum theory on the basis of which the simulation procedures were written. The quantum model of energy transfer in PSIIRC that was used to generate the target functions is explained in the fifth section. The results of the strategy test for different settings of DE and full datasets of the fitting procedure for two different strategies are given in section six. Finally, some features of the strategy test, the algorithm convergence at different DE settings, and further perspectives of DE application for the modeling of primary photosynthetic processes are discussed in section seven.

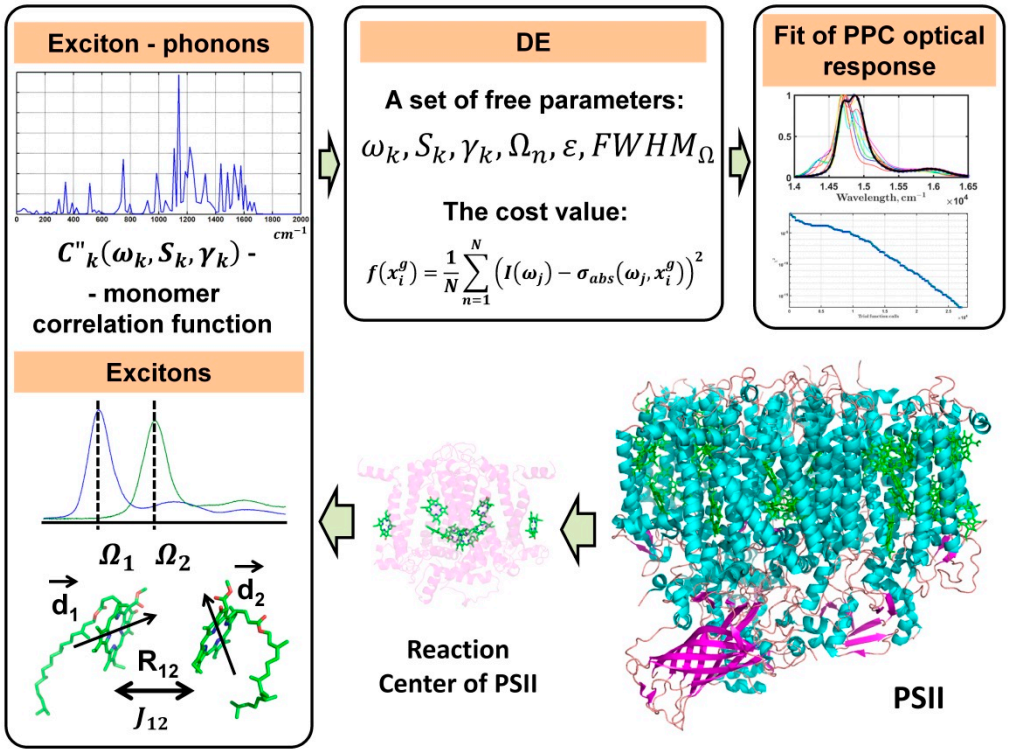

Figure 1. Scheme of the PPC linear optical response fitting procedure. The crystal structure of photosystem II and the isolated reaction center are shown at the bottom of the figure. The left block represents the employed theories in the simulation: the exciton theory (transition energies Ω_n, transition moments d_n, distances between the centers of transition moments R_{nm}, coupling energies J_{nm}, the dielectric constant ε, the full width at half maximum of inhomogeneous broadening $FWHM_\Omega$) and the multimode Brownian oscillator model ($\{\omega_j, S_j, \gamma_j\}$ are frequencies, the Huang–Rhys factors, and damping factors of a vibronic mode). The upper blocks symbolize the differential evolution fitting procedures ($I(\omega_n)$ is a measured spectrum, $\sigma_{abs}\left(\omega_n, \mathbf{x}_i^g\right)$ is a simulated spectrum). See more detailed explanations in the text.

2. Statement of the Optimization Problem

Using of the molecular exciton theory in modeling the optical properties of a PPC from a mathematical point of view is the sequential implementation of computational procedures such as matrix diagonalization, fast Fourier transform, and numerical integration of time- and frequency-dependent functions. Depending on the characteristics of the vibronic modes of the correlation functions, the number of pigments in the complex, and the interaction energies between them, the speed and quality of the calculated spectra can vary significantly. In general (Figure 1), a set of parameters $x_j = \{\omega_k, S_k, \gamma_k, \Omega_n, \varepsilon, FWHM_\Omega\}$ is fed to the input of the simulation program, which entirely determines the simulated spectra of the complexes. This set, with which the spectra are calculated, we will hereafter refer to as a solution of the PSIIRC optical response modeling. Since the exciton theory is semiclassical and does not assume ab initio calculations, in order to find x_j, it is necessary to compare the calculated spectra with those measured experimentally. Thus, by varying the values of x_j, one can try to find a solution for which the calculated spectra most accurately describe the measured ones. Ideally, the best solution is the set that corresponds to the exact coincidence of the calculated and measured spectra.

The dependence of the calculated spectra on x_j is very complex and cannot be factorized. Many publications are devoted to the search "manually" for a set of x_j for the PSIIRC exciton model and almost always use the simultaneous simulation of several spectra obtained by different experimental techniques. For example, in the paper by Novoderezhkin et al. [32], four exciton models of energy transfer in PSIIRC are considered, which correspond to four

different sets of x_j. It is clear that the process of finding a set of model parameters that would allow the most accurate fit of the calculated and measured spectra can be optimized. Evolutionary algorithms are applicable for this purpose if we consider the squared difference between the calculated and experimental spectra as an objective function to be minimized. The use of DE in this case is preferable to genetic algorithms, since it allows for varying the parameters continuously instead of discretely. Moreover, DE allows us to classify the found solutions x_j with respect to the value of the objective function. The smallest value of the objective function corresponds to the smallest difference between the calculated and experimental spectra. Of course, the algorithm may become stuck in the local minimum, when any changes in x_j within certain values x_j^{local} make the objective function only worse and convergence stagnates.

Thus, the combined software implementation of the optical response modeling procedures and the differential evolution algorithm will make it possible to find the exciton model parameters that will provide the best match between the experimental and computational data.

3. Differential Evolution

The algorithm of DE has four data processing steps: initialization, mutation, crossover, and selection. The initialization of DE runs once at the beginning of the fitting, while three other steps sequentially repeat themselves as many times as required to obtain the appropriate simulated spectra (Figure 1).

At the initialization of DE, a matrix of model parameters, $\mathbf{X}$, is filled with random values within specified limits, and then the objective function values are estimated. The size of the matrix is $D \times N_p$, where D is equal to the number of model parameters, and N_p is the size of the population. Assuming that x_i are the parameters to find, $j = 1, 2, \ldots, D$ and $\mathbf{x} = x_j$, then the matrix of model parameters is written as $\mathbf{X} = \mathbf{x}_i$, where $i = 1, 2, \ldots, N_p$. The elements of the matrix are chosen taking into account the boundary conditions, which consider the physical limits of the parameters to find.

After the initialization step, the main cycle of DE starts with the generation of a new matrix, $\mathbf{X}^g$, where $g = 0, 1, \ldots, g_{max}$ is a generation index. In the classical version of DE, a mutant vector, $\mathbf{v}_i^g$, is calculated according to one of the following five expressions:

$$\mathbf{v}_i^g = \mathbf{x}_{r0}^g + F\left(\mathbf{x}_{r1}^g - \mathbf{x}_{\mathrm{r2}}^g\right), \tag{1}$$

$$\mathbf{v}_{\mathrm{i}}^g = \mathbf{x}_{best}^g + F\left(\mathbf{x}_{r1}^g - \mathbf{x}_{r2}^g\right), \tag{2}$$

$$\mathbf{v}_i^g = \mathbf{x}_i^g + F\left(\mathbf{x}_{best}^g - \mathbf{x}_{r0}^g\right) + F\left(\mathbf{x}_{r1}^g - \mathbf{x}_{r2}^g\right), \tag{3}$$

$$\mathbf{v}_i^g = \mathbf{x}_{best}^g + F\left(\mathbf{x}_{r1}^g - \mathbf{x}_{r2}^g\right) + F\left(\mathbf{x}_{r3}^g - \mathbf{x}_{r4}^g\right), \tag{4}$$

$$\mathbf{v}_i^g = \mathbf{x}_{r0}^g + F\left(\mathbf{x}_{r1}^g - \mathbf{x}_{r2}^g\right) + F\left(\mathbf{x}_{r3}^g - \mathbf{x}_{r4}^g\right), \tag{5}$$

where F is the weighting factor and $F \in [0, 1]$; $\mathbf{x}_i^g$, $\mathbf{x}_{r0}^g$, $\mathbf{x}_{r1}^g$, and $\mathbf{x}_{r2}^g$ are randomly chosen vectors from the current population; and $(i \neq r0 \neq r1 \neq r2) \in [0, Np]$. $\mathbf{x}_{best}^g$ is a vector corresponding to the best solution (minimum of the objective function).

The diversity of the trial vector population can be increased by applying a crossover procedure. In this case, a new trial vector, $\mathbf{u}_j^g$, is created by exchanging the elements of each target vector of the current population with those of a mutant one. The crossover rate, $Cr \in [0, 1]$, determines the number of exchanged values in the trial vector. There are two types of crossovers: binomial and exponential. The combination of Equations (1)–(5) and 2 crossovers provides us with 10 different strategies to create a new generation of model parameters. The names of the strategies are formed as follows: DE/x/y/z, where x is a base vector (*rand*, *best*, *rand-to-best*), y is the number of differences (1 or 2), and z is the

crossover type (*exp* or *bin*). Thereby, the convergence of the algorithm can be controlled by choosing the optimal strategy and varying the weighting factor and crossover rate.

Thus, the target vector of a new generation, g + 1, is determined by comparing $f\left(\mathbf{u}_i^g\right)$ and $f\left(\mathbf{x}_i^g\right)$. The expression for the objective function $f\left(\mathbf{x}_i^g\right)$ is:

$$f\left(\mathbf{x}_i^g\right) = \frac{1}{N}\sum_{n=1}^{N}\left(I(\omega_n) - \sigma_{abs}\left(\omega_n, \mathbf{x}_i^g\right)\right)^2, \tag{6}$$

where $I(\omega_n)$, for example, is a measured absorption spectrum of PSIIRC at frequency ω_n, $\sigma_{abs}\left(\omega_n, \mathbf{x}_i^g\right)$ is a simulated absorption spectrum of PSIIRC, and N is the number of points in the spectra. After the objective functions are evaluated, $\mathbf{x}_i^{g+1}$ vector allocation is made according to the following conditions:

$$\mathbf{x}_i^{g+1} = \begin{cases} \mathbf{u}_i^g, & f\left(\mathbf{u}_i^g\right) \le f\left(\mathbf{x}_i^g\right) \\ \mathbf{x}_i^g, & f\left(\mathbf{u}_i^g\right) > f\left(\mathbf{x}_i^g\right) \end{cases}, \tag{7}$$

When a new population is completed, the next cycle of DE starts, and the optimization runs until the predetermined minimum of the objective function is reached or the number of generations reaches a specified maximum.

4. Theory

4.1. Multimode Brownian Oscillator Model

According to quantum theory of the radiation interaction with matter, the optical response of any pigment molecule can be estimated by expanding the expression for the polarization of a system, $P(t)$, in powers of the radiation field assuming this field as a perturbation. Consider a system of two electronic states: a ground state $|g\rangle$ and an excited one $|e\rangle$, and let $\mu_{eg}(\mathbf{q})$ be a transition dipole moment between states. Then, the polarization can be written as the expectation value of $\mu(\mathbf{q})$:

$$P(\mathbf{r}, t) = Tr\left[\left(\mu_{eg}(\mathbf{q})|e\rangle\langle g| + \mu_{ge}(\mathbf{q})|g\rangle\langle e|\right)\rho(t)\right], \tag{8}$$

where $\rho(t)$ is a density matrix whose time evolution is determined by the Hamiltonian of the system. The expansion of $\rho(t)$ in powers of the field results in the decomposition of polarization $P(\mathbf{r}, t) = P(\mathbf{r}, t)^{(1)} + P(\mathbf{r}, t)^{(2)} + P(\mathbf{r}, t)^{(3)} + \cdots$. The first term $P(\mathbf{r}, t)^{(1)}$ of this decomposition is responsible for the linear absorption:

$$P(\mathbf{r}, t)^{(1)} = -\frac{i}{\hbar}\int_0^\infty dt_1 E(\mathbf{r}, t - t_1) S^{(1)}(t_1), \tag{9}$$

where $S^{(1)}(t_1) = \frac{i}{\hbar}\theta(t_1)\langle\mu_{eg}(t_1)\mu_{eg}(0)\rho(-\infty)\rangle + c.c.$ is the linear response function in the Liouville representation, $E(\mathbf{r}, t)$ is the radiation field, $\theta(t_1)$ is the Heaviside step function, and $\langle\ldots\rangle$ denotes the averaging over nuclear degrees of freedom, $t_1 = \tau_2 - \tau_1$, where τ_i are the ordered points on $[t_0, t]$ used in the decomposition of polarization. A general expression for an absorption spectrum can be written in an integral form:

$$\sigma_{abs}(\omega) = \int_{-\infty}^{\infty} dt\ S^{(1)}(t_1) e^{i\omega t}, \tag{10}$$

Introducing the effective operator of the electronic energy gap, $U(\tau) = \exp\left(\frac{i}{\hbar}H_g\tau\right)U \exp\left(-\frac{i}{\hbar}H_g\tau\right)$, where $U = H_e(\mathbf{q}) - H_g(\mathbf{q}) - \hbar\omega_{eg}$, $H_e(\mathbf{q})$, and $H_g(\mathbf{q})$ are Hamiltonians of

the electronic excited and ground states, and ω_{eg} is an arbitrary parameter. Considering the time evolution of $U(\tau)$, the first order response function [13] can be expressed as:

$$S^{(1)}(t_1) = \frac{i}{\hbar}\theta(t_1)e^{-i\omega_{eg}t_1 - g(t_1)} + c.c., \tag{11}$$

$$g(t) = \int_0^t d\tau_2 \int_0^{\tau_2} d\tau_1 C(\tau_1), \tag{12}$$

$$C(\tau_1) = \frac{1}{\hbar^2}\langle U(\tau_1)\, U(0)\rho_g\rangle, \tag{13}$$

where $g(t)$ is the lineshape function; $C(\tau_1)$ is the two-time correlation function of $U(\tau)$. Since the correlation function is complex, it can be expressed in the time domain as $C(t) = C'(t) + C''(t)$, and as $C(\omega) = \int_{-\infty}^{\infty} dt\, e^{i\omega t}C(t) = C'(\omega) + C''(\omega)$ in the frequency domain. Considering the fluctuation dissipation theorem, we obtain the expression for $C(t)$ in the following form:

$$C(t) = \int_{-\infty}^{\infty} d\omega\ \cos(\omega t)\coth(\beta\hbar\omega/2)C''(\omega) + i\int_{-\infty}^{\infty} d\omega\ \sin(\omega t)C''(\omega), \tag{14}$$

where $C''(\omega)$ is the imaginary part of $C(\omega)$ and can be treated classically. This feature of $C''(\omega)$ makes it quite suitable for the modeling of the optical response. Thus, the equation for $g(t)$ in terms of $C''(\omega)$ is written as:

$$g(t) = \frac{1}{2\pi}\int_{-\infty}^{\infty} d\omega \frac{1-\cos\omega t}{\omega^2}\coth(\beta\hbar\omega/2)C''(\omega) - \frac{i}{2\pi}\int_{-\infty}^{\infty} d\omega \frac{\sin(\omega t) - \omega t}{\omega^2}C''(\omega). \tag{15}$$

Taking into account Equations (10) and (11), the final expression for numerical simulation of the absorption lineshape is given by:

$$\sigma_{abs}(\omega) = \frac{1}{\pi}Re\ \int_0^{\infty} dt\ e^{i(\omega-\omega_{eg})t}e^{-g(t)}. \tag{16}$$

The combination of Equations (15) and (16) allow for the modeling of the linear optical response of a single electronic transition interacting with an arbitrary set of vibronic modes.

In order to evaluate $C''(\omega)$, the theory of MBOM must be applied [13]. In terms of MBOM, a system consisting of an electronic state interacting with a set of vibronic states is described by the following Hamiltonians:

$$H_{sys} = H_g + H_e + H_{VB}, \tag{17}$$

$$H_g = \sum_j^N \left(\frac{p_j^2}{2m_j} + \frac{1}{2}m_j\omega_j^2 q_j^2\right), \tag{18}$$

$$H_e = \hbar\omega_{eg}^0 + \sum_j^N \left(\frac{p_j^2}{2m_j} + \frac{1}{2}m_j\omega_j^2 (q_j + d_j)^2\right), \tag{19}$$

$$H_{VB} = \sum_n^M \left[\frac{p_n^2}{2m_n} + \frac{1}{2}m_n\omega_n^2 x_n^2 - x_n\sum_j c_{nj}q_j + \frac{\sum_j c_{nj}^2 q_j^2}{2m_n\omega_n^2}\right], \tag{20}$$

where H_g and H_e are Hamiltonians of the ground $|g\rangle$ and the excited $|e\rangle$ states. Vibronic states of the system are modeled by introducing a certain number of effective vibronic modes. Each mode is characterized by frequency ω_j, mass m_j, momentum p_j, coordinate q_j, and displacement d_j of the excited state potential curve. j is the index of a mode, and N is the number of modes. The influence of the local environment is represented by the H_{VB} part in the system Hamiltonian, which depends on another set of oscillators, the bath modes, and their parameters $\{p_n, x_n, \omega_n, m_n\}$. The coupling between electronic and vibronic states

is set by microparameters c_{nj}. Finally, the MBOM correlation function is calculated using the path integral method. The imaginary part of $C(t)$ is written in the form:

$$C''(\omega) = \sum_j \frac{2S_j\omega_j^3\omega\gamma_j}{\left(\omega_j^2 - \omega^2\right)^2 + \omega^2\gamma_j^2}, \tag{21}$$

where $S_j = d_j^2/2$ are the Huang–Rhys factors, and γ_j are the damping factors for each ω_j that are determined empirically.

So, to calculate the absorption or the fluorescence spectrum of a monomeric pigment molecule, such as chlorophyll, bacteriochlorophyll, or carotenoid, both in solvent and in protein, one has to evaluate the spectral density (Equation (21)) then the lineshape function (Equation (15)), and the absorption lineshape is simulated according to Equation (16).

4.2. Excitons

In the previous section, it was shown how to model the linear optical response of a monomeric pigment. The theory of molecular excitons considering electronic transition and interaction energies between pigment molecules of PSIIRC allows calculating the contributions of each Chl molecule to the resulting spectra and population kinetics [16,30,34,35]. We consider that PSIIRC consist of eight two-level Chl molecules; each molecule can be either in a ground $|0\rangle$ or in an excited $|n\rangle$ state. n runs from *1* to N, where N is the number of pigments in PSIIRC. Denoting $B_n^+ = |n\rangle\langle 0|$ as the exciton creation operator and $B_n = |0\rangle\langle n|$ as that of annihilation, the PSIIRC exciton Hamiltonian is then written in the form:

$$H_{ext} = \sum_n \Omega_n B_n^+ B_n + \frac{1}{2}\sum_{n\neq m} J_{mn}\left(B_m^+ B_n + B_n^+ B_m\right), \tag{22}$$

where Ω_n is the transition energy between the ground and the excited states of a pigment. B_n^+ and B_n obey the commutation rules $[B_n, B_n^+] = 1$. J_{mn} is a matrix of coupling energies calculated employing the extended dipole approximation [36]. This method of calculating the interaction energies using the values of partial charges is much more accurate than the classical dipole–dipole approximation.

Diagonalizing the Hamiltonian (Equation (22)), we obtain the eigenstates c_n^α and eigenvalues ϵ_α that allow for the transformation of the system parameters from the site representation to the exciton representation. Thereby, the lineshape function (Equation (15)) in the exciton representation is $g_{\mu\nu\alpha\beta}(t) = \sum_{mnkl} c_m^\mu c_n^\nu c_k^\alpha c_l^\beta g_{mnkl}(t)$, where $\alpha, \beta, \ldots = 1 \ldots N$ are indices of the exciton states. Finally, the expressions for exciton absorption, circular and linear dichroism, and fluorescence spectra will be presented as a sum over exciton states [9,36]:

$$\sigma_{abs}^{ext}(\omega) \approx \frac{\omega}{\pi}\sum_\alpha^N \mathbf{d}_\alpha^2 Re\int_0^\infty dt e^{i(\omega-\epsilon_\alpha)t} e^{-g_{\alpha\alpha\alpha\alpha}(t)} e^{-0.5K_{\alpha\alpha}t} \tag{23}$$

$$\sigma_{CD}^{ext}(\omega) \approx \frac{\omega}{\pi}\sum_\alpha^N \mathbf{R}_\alpha Re\int_0^\infty dt e^{i(\omega-\epsilon_\alpha)t} e^{-g_{\alpha\alpha\alpha\alpha}(t)} e^{-0.5K_{\alpha\alpha}t} \tag{24}$$

$$\sigma_{LD}^{ext}(\omega) \approx \frac{\omega}{\pi}\sum_\alpha^N \left[d_\alpha^{z2} - \frac{1}{2}\left(d_\alpha^{x2} + d_\alpha^{y2}\right)\right] Re\int_0^\infty dt e^{i(\omega-\epsilon_\alpha)t} e^{-g_{\alpha\alpha\alpha\alpha}(t)} e^{-0.5K_{\alpha\alpha}t} \tag{25}$$

$$\sigma_{fl}^{ext}(\omega) \approx \frac{\omega^3}{\pi}\sum_\alpha^N \frac{(\mathbf{nd}_\alpha)^2 e^{\epsilon_\alpha\beta}}{\sum_n e^{\epsilon_\alpha\beta}} Re\int_0^\infty dt e^{i(\omega-\epsilon_\alpha+2\lambda_{\alpha\alpha\alpha\alpha})t} e^{-g_{\alpha\alpha\alpha\alpha}{}^*(t)} e^{-0.5K_{\alpha\alpha}t}, \tag{26}$$

where $\lambda_{\alpha\alpha\alpha\alpha} = -\lim_{\tau\to\infty} Im\left[\frac{dg_{\alpha\alpha\alpha\alpha}(\tau)}{d\tau}\right]$ is the reorganization energy of an exciton state α; $K_{\alpha\alpha} = \sum_{\beta} K_{\alpha\beta}$ are the exciton relaxation rates; $\mathbf{d}_\alpha = \sum_n c_n^\alpha \mathbf{d}_n$ is the Q_y transition moments of Chl transformed to the exciton representation; and $\mathbf{R}_\alpha = \sum_{nm} c_n^\alpha c_m^\alpha r_{nm}(\mathbf{d}_n \times \mathbf{d}_m)$ is a matrix of the rotational strength necessary for CD spectra simulation.

5. Exciton Model of the Photosystem II Reaction Center

PSIIRC is an important PPC of photosystem II of higher plants and cyanobacteria. All of the light quanta energy absorbed by photosynthetic PPC with minimum losses eventually transfers to the reaction centers where chemical reactions of charge separation occur. In addition to being the location of chemical reactions, reaction centers actively serve as a light-harvesting complex, too. PSIIRC has six Chls, two pheophytins, and two carotenoids, which absorb at the visible range. In this study, we are going to model the PSIIRC optical response only in the so-called Q_y region of Chl absorption which corresponds to the 650–750 nm range. It means that the excited states of carotenoids will not be taken into account in the exciton Hamiltonian (Equation (22)). Since our simulations are focused only on the linear spectroscopy (absorption, steady-state fluorescence, circular and linear dichroism), the radical pair states are not considered. Thus, the PSIIRC exciton Hamiltonian in our modeling will include contributions of eight pigments: two Chls of the special pair (PD1 and PD2), two accessory Chls, two pheophytins, and two peripheral Chls (Figure 2B).

To explore the potential of DE as an effective optimization procedure for fitting the PSIIRC spectra, we will use the simulated experimental data instead of the measured ones. The real data are always noisy and may contain some inconspicuous contributions that can only worsen the convergence of the optimization. The simulated experimental data as target functions will allow the algorithm, in the case of successful configuration, to converge almost to machine zero and determine the local minima for parameters of the PSIIRC quantum model.

To simulate the optical response of Chl, we used the results of our previous studies. The spectral density, absorption, and fluorescence spectra of monomeric Chl are shown in Figure 2A. However, to take into account that the surrounding of Chls in PSIIRC is different from that of it in solution, we used special values of $\{\omega_{low}, S_{low}, \gamma_{low}\}$ determined previously for the lowest vibronic mode. The total number of vibronic modes in Equation (21) was 39. The number of points in the time and frequency arrays was defined as $n = 2^{11} = 2048$. The time step of integration was 0.0042 ps. The full set of $\{\omega_j, S_j, \gamma_j\}$ for Chl can be found in our previous publications [9,23].

Parameters of the PSIIRC exciton model are shown in Table 1. The energies of the Q_y transition of Chls and pheophytins were chosen in such a way that the simulated linear spectra, according to Equations (16)–(20), were as close as possible to the measured ones at room temperature. The interaction energies between PSIIRC cofactors were calculated in the extended dipole approximation, except for the coupling between Chls in the special pair; according to the previous studies, it was set as 150 cm^{-1}. It must be stressed that the inhomogeneous broadening $FWHM_\Omega$ [9] was not taken into account in the simulations, since it requires averaging over random perturbations of diagonal elements of the exciton Hamiltonian (Equation (22)). We deliberately made such a simplification in order to allow the algorithm of DE to converge to machine zero. The Q_y transition moments and the spectral densities of Chl and pheophytin are slightly different and when modeling the real experimental data, these distinctions must be accounted for; however, for the purposes of this study, it is enough to consider them to be equal. As a result, the calculated spectra of absorption, steady-state fluorescence, and linear and circular dichroism we used for the strategy tests and for optimization with the maximum number of free parameters are presented in Figure 2B.

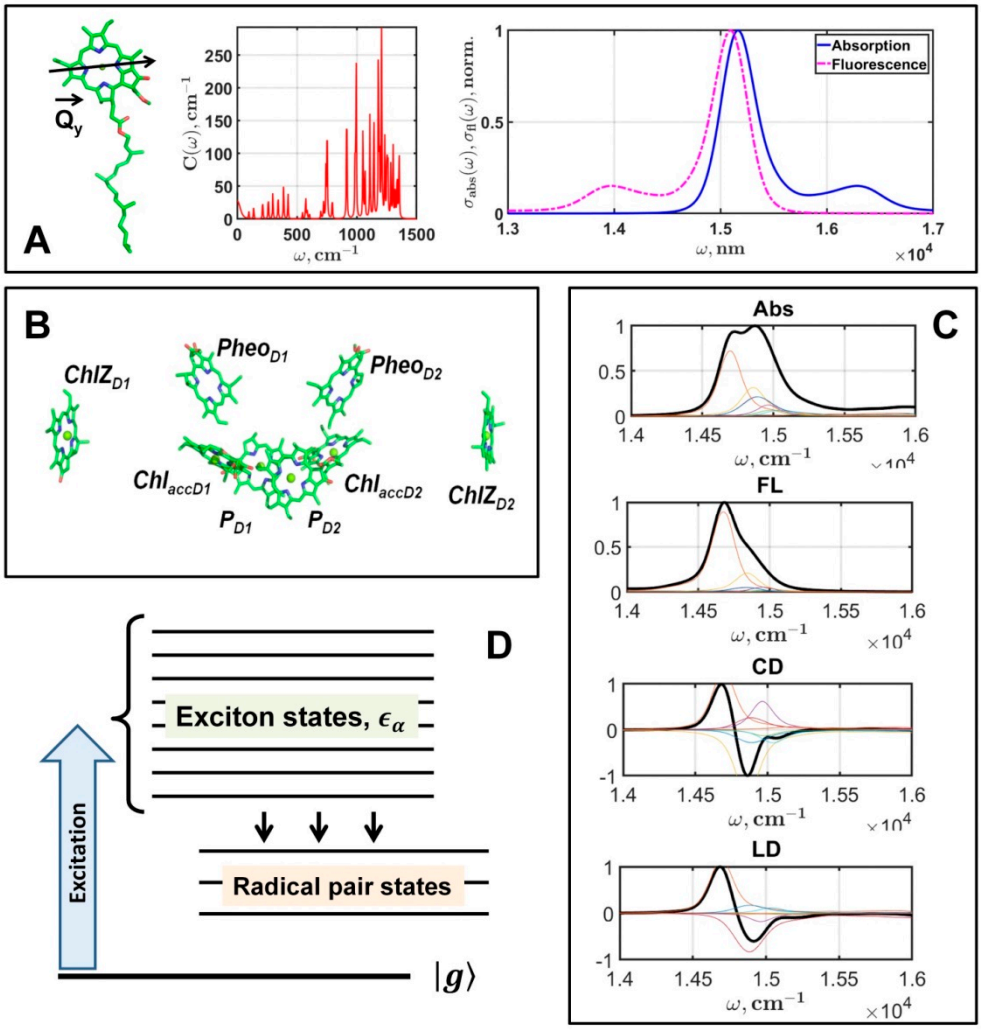

Figure 2. Optical properties of monomeric Chl, the main pigment of Photosystem II reaction center: the spectral density (red) of Chl and the simulated absorption (blue) and fluorescence spectra (magenta) of Chl (**A**); the mutual orientation of Photosystem II reaction center cofactors (**B**) is a key factor in the exciton theory (a scheme (**D**) of the energy levels of PSIIRC) that was applied to simulate absorption, circular and linear dichroism, and steady-state fluorescence spectra. These spectra were used as the target functions (**C**).

Table 1. Material Hamiltonian of the PSIIRC exciton model used for simulation of target functions.

	PD1	**PD2**	**Chl$_{acc}$D1**	**Chl$_{acc}$D2**	**PheoD1**	**PheoD2**	**Chl$_Z$D1**	**Chl$_Z$D2**	**Ω_n**
PD1	0	150.00	−30.94	−100.96	−3.91	19.01	0.74	0.96	14,960.0
PD2		0	−96.75	−23.53	24.53	−4.22	1.11	1.06	15,070.0
Chl$_{acc}$D1			0	12.43	60.92	−4.96	2.98	0.03	15,045.0
Chl$_{acc}$D2				0	−5.80	54.97	−0.02	2.71	15,080.0
PheoD1					0	3.10	−4.06	−0.32	15,100.0
PheoD2						0	−0.29	−4.44	15,120.0
Chl$_Z$D1							0	0.24	15,180.0
Chl$_Z$D2								0	15,170.0

6. Results

6.1. Strategy Test

According to our previous modeling of the linear absorption of monomeric chlorophylls, bacteriochlorophylls, and carotenoids, *DE/rand-to-best/1/exp* and *DE/best/1/bin* strate-

gies have demonstrated the best convergence rates. Preliminary trial runs of the optimization algorithm for the PSIIRC complex showed that, in general, the results of convergence are similar to those we obtained for monomeric pigments. Thus, in the case of PSIIRC, it was decided to run a strategy test only for the two best DE classical strategies. The strategy control parameters varied from 0.55 to 0.85 for F and from 0.8 to 1.0 for Cr with a discrete step of 0.05.

The number of free parameters required to simulate the linear optical response of PSIIRC without inhomogeneous broadening is 12:8 Q_y transition energies Ω_n for Chls and pheophytins, the effective dielectric constant, which is used to calculate the coupling energies between pigments, and 3 parameters $\{\omega_{low}, S_{low}, \gamma_{low}\}$ for the lowest vibronic mode in the spectral density. To reduce the calculation time and to more clearly demonstrate the effect of convergence, only 5 of the 12 PSIIRC model parameters were set as free during the fitting procedure: 4 transition energies and the dielectric constant. Moreover, fewer free parameters allow the optimization algorithm to converge in fewer generations. So, we set $g_{max} = 50$ and performed 30 runs of the program for each $\{F, Cr\}$ pair. The results of the strategy test are shown in Figure 3A,B.

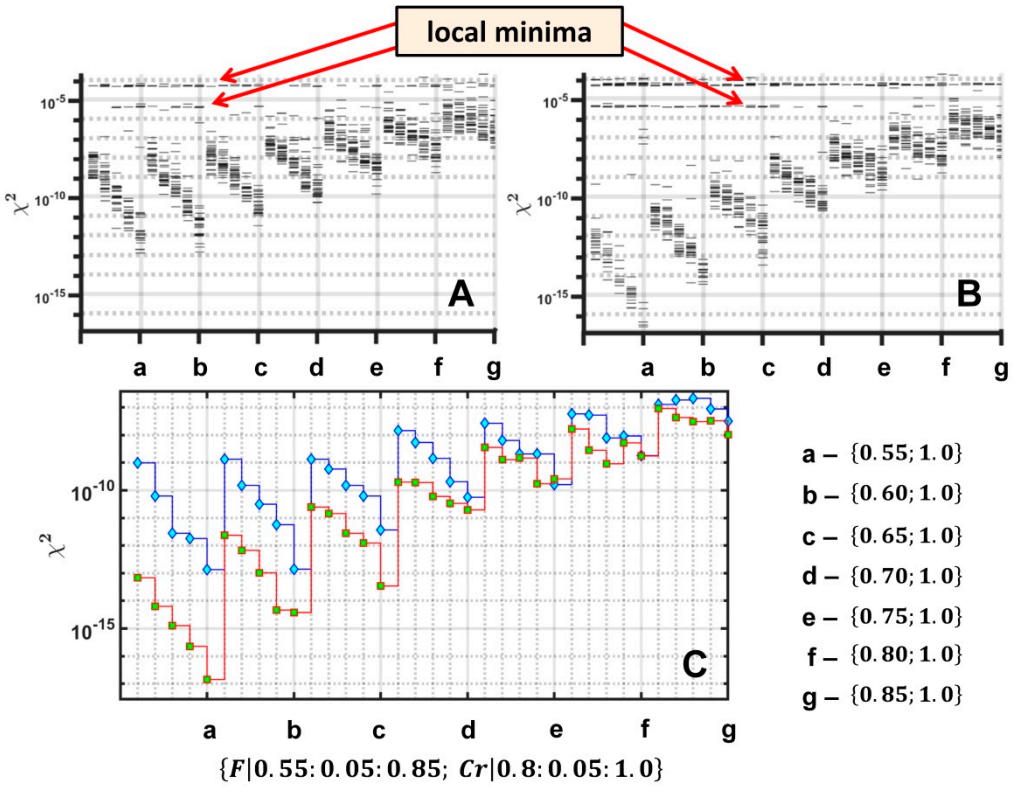

Figure 3. Strategy test. Distributions of the objective functions values obtained for *DE/best/1/bin* (**A**) and *DE/rand-to-best/1/exp* (**B**) strategies after 30 runs of DE for each $\{F, Cr\}$ pair. Comparison of the best results for *DE/best/1/bin* (blue) and *DE/rand-to-best/1/exp* (red) are shown in plot (**C**). Latin letters correspond to $\{F, Cr\}$ pairs. Red lines indicate the local minima of optimization.

Figure 3C demonstrates the best values of the objective function obtained for two strategies. The plots show that the optimization becomes stuck in at least in two minima. Thus, it can be argued that if the value of objective function is less than the lowest local minimum, which is equal to 4.37472×10^{-7}, the algorithm finds the best solution and does not stick at any local minima. Taking into account this criterion, the number of successful optimizations for all $\{F, Cr\}$ pairs and two strategies was calculated. These data are shown in Tables 2 and 3.

Table 2. The results of the strategy test. The number of successful optimizations of PSIIRC fitting after 30 runs of DE for each $\{F;\ Cr\}$ pair and the *DE/rand-to-best/1/exp* strategy.

F	***Cr***				
	0.8	**0.85**	**0.9**	**0.95**	**1**
0.55	29	25	27	24	21
0.60	27	27	25	24	23
0.65	29	27	28	26	25
0.70	28	30	28	28	28
0.75	30	28	30	28	25
0.80	27	29	28	26	25
0.85	19	23	25	24	27

Table 3. The results of the strategy test. The number of successful optimizations of PSIIRC fitting after 30 runs of DE for each $\{F;\ Cr\}$ pair and the *DE/best/1/bin* strategy.

F	***Cr***				
	0.8	**0.85**	**0.9**	**0.95**	**1**
0.55	20	14	9	18	9
0.60	24	24	23	22	17
0.65	21	23	22	17	24
0.70	22	26	23	24	22
0.75	27	29	26	26	23
0.80	25	24	24	24	25
0.85	24	28	26	25	26

To compare the effectiveness of the two strategies, we calculated the percentage of convergence, taking into account the criterion of the lowest local minimum. The convergence probability for *DE/rand-to-best/1/exp* strategy is 87.9% (923 of 1050) and 74.9% (786 of 1050) for *DE/best/1/bin*.

6.2. PSIIRC Linear Optical Response Modeling

To perform the optimization of PSIIRC linear optical response modeling, we tuned the DE algorithm based on the values of convergence rates and convergence probabilities obtained in the strategy test. Considering the results of the strategy test, the corresponding values $\{F = 0.55, Cr = 0.9\}$ were chosen. Unlike the strategy test, the number of free parameters was nine. All of the excitation energies Ω_n were set free, as well as the dielectric constant. The initial boundaries for Ω_n were from 14,500 cm^{-1} to 15.300 cm^{-1} and from 0.5 to 2 for the dielectric constant, ε.

For greater accuracy and more detailed information about the convergence dynamics, the maximum number of generations g_{max} chosen was 300. The results of the PSIIRC linear optical response fitting for the two strategies are shown in Figures 4 and 5. As we can see, the *DE/rand-to-best/1/exp* strategy found the best solution as opposed to *DE/best/1/bin* which stuck at local minimum.

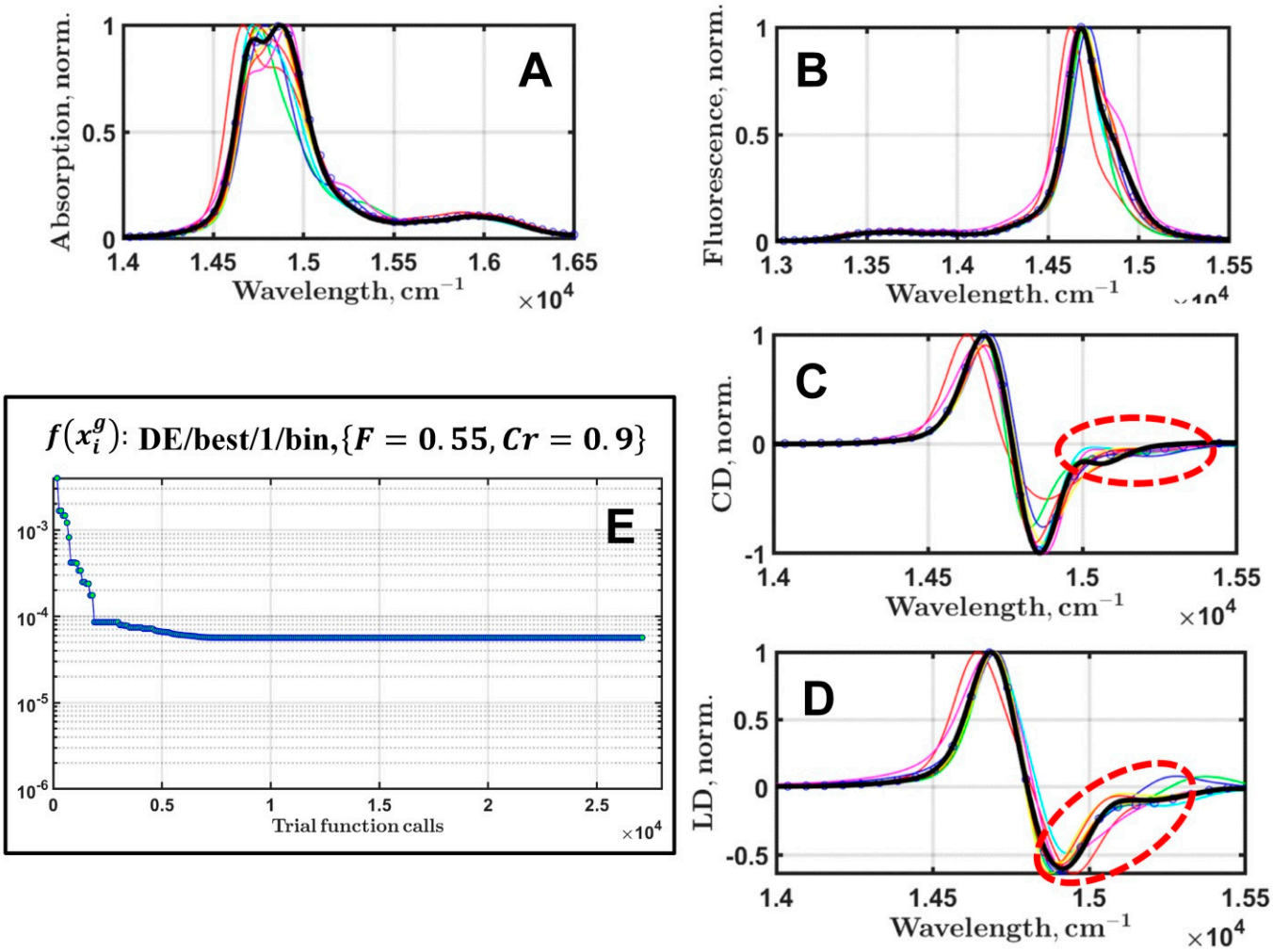

Figure 4. Results of the PSIIRC linear optical response fitting. The case when DE is stuck in a local minimum. *DE/best/1/bin* strategy. The best simulated spectra (black lines with circular markers) of absorption (**A**), steady-state fluorescence (**B**), circular (**C**), and linear (**D**) dichroism are shown. Color lines are the spectra found by DE after first 7 generations. Black thick lines are the target spectra. Red ovals indicate those parts of the spectra where there are significant discrepancies between the target spectra and those found by DE. The objective function $f\left(\mathbf{x}_i^g\right)$ dependence on the number of the trial function (linear response simulation) calls (**E**).

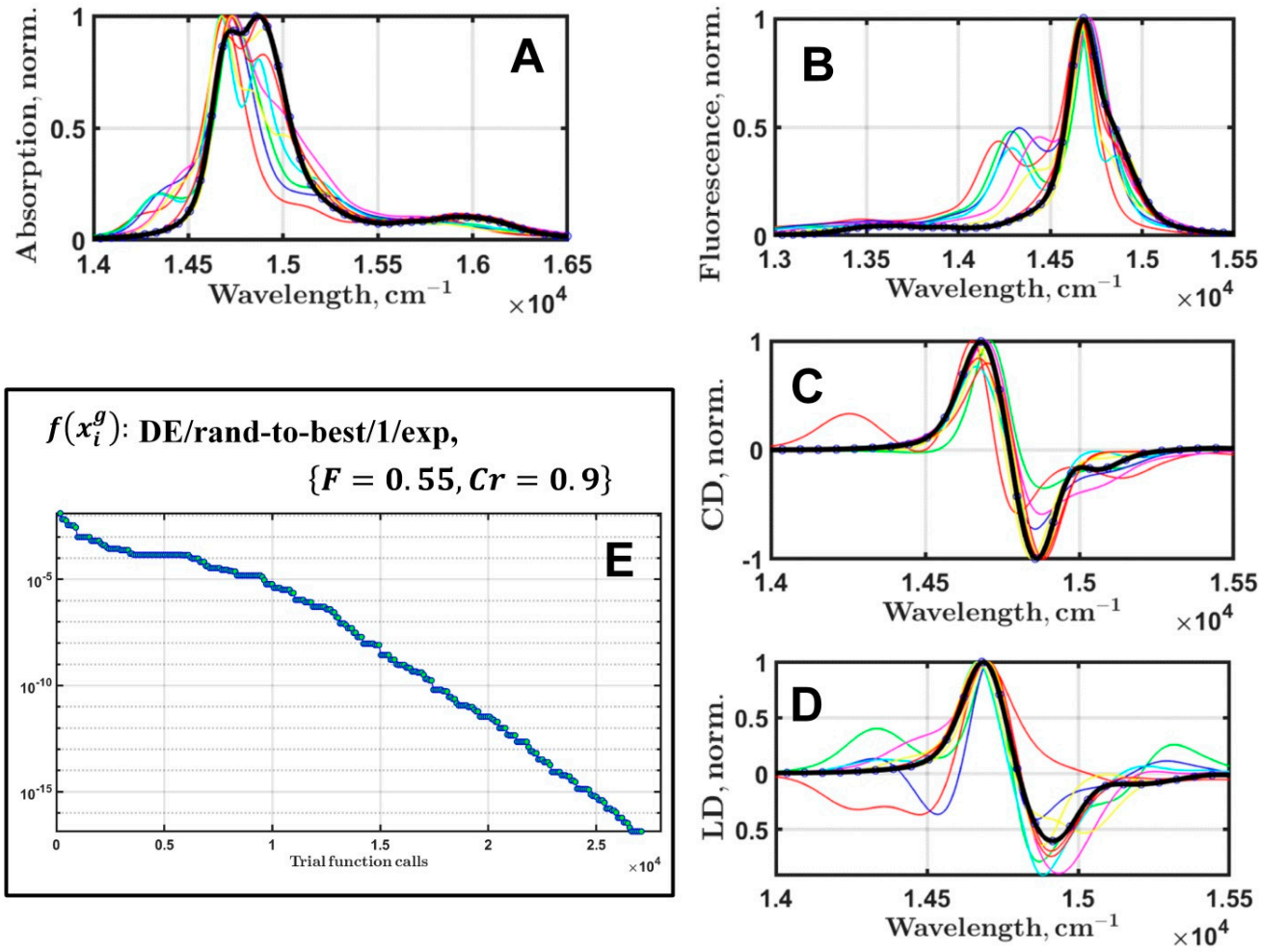

Figure 5. Results of the PSIIRC linear optical response fitting. Successful DE run. *DE/rand-to-best/1/exp* strategy. The best simulated spectra (black lines with circular markers) of absorption (**A**), steady-state fluorescence (**B**), circular (**C**), and linear (**D**) dichroism are shown. Color lines are the spectra found by DE after first 7 generations. Black thick lines are the target spectra. The objective function $f\left(\mathbf{x}_i^g\right)$ dependence on the number of the trial function (linear response simulation) calls (**E**).

7. Discussion

Some attempts to use the evolutionary multiparametric optimization for modeling the optical properties of PPC have already been made. The genetic algorithm was used to estimate the charge and energy transfer rates in photosystem I core complexes [37]. However, this first effort was not really successful: linear spectra and kinetics were not simulated; only transfer rates were calculated to compare with those measured. Moreover, the protein crystal structure was not available at that moment, which significantly limited the proper use of exciton theory. The later attempt employing the same approach was used for the light-harvesting complex II from higher plants [38]. In this case, some parameters of the exciton model were estimated, taking into account the existing crystal structure, but the overall optimization approach based on two-dimensional lattice model appeared to be not very effective.

PPCs with a large number of pigments are the perfect objects for testing the effectiveness of optimization algorithms. Simulating PPC optical properties requires considering the electronic transition energies of all pigments in PPCs [2]. The exciton spectra of photosystem I from *Synechococcus elongatus* [39] were simulated with the help of the genetic algorithm. The monomeric complex of photosystem I is characterized by a large number of Chls, about 100 per complex. The main drawback of this study is the simulation of linear

optical response as "stick" spectra, which is a rough approximation of the spectrum widths for such PPCs. However, transition energies were modeled using a variation of genetic algorithm. For each pigment, the Q_y transition energy could vary discretely within the interval of 660–715 nm with a step of 0.25 nm. Such a discretization of the parameters to search is the main disadvantage of the genetic algorithm in comparison with DE.

Another interesting example of the modeling of the exciton dynamic, linear spectra and time-resolved fluorescence of the monomeric photosystem I, applying a certain mutation strategy of genetic algorithm, is described in [40]. The spectra of individual excitonic states were simulated in terms of the Redfield relaxation theory, which already makes it possible to estimate the width of each exciton state depending on its energy. A different protein environment around Chls creates variations in the Q_y transition energies, which cannot be estimated theoretically. The use of evolutionary optimization in this case is one of the ways to solve the problem of finding Q_y transition energies without resorting to tedious quantum mechanical calculations. The authors of [40] proposed several mutation strategies of the genetic algorithm for searching for transition energies; however, due to the huge search space, the algorithm did not achieve a correct assignment of most Chl energies.

In our simulations of the linear spectra of PSIIRC, we applied the modified Redfield theory [35] (actually, a combination of MBOM and the exciton theory) to calculate the absorption profile for each exciton state (Equations (23)–(26)). This approach allows us to reproduce very realistic spectra for each exciton state of PSIIRC. Chls and Pheos in PSIIRC are characterized by a set of *39* vibronic modes, which gives the advantage in modeling the effect of electron–phonon interaction compared with the standard Redfield approach. However, in applying this complex approach, we increase the number of free model parameters, which in turn increases the computational costs of the experimental data fitting. Our previous studies of the linear optical response of Chl, BChl, and carotenoids in solutions were modeled considering MBOM theory [4,22,23]. To overcome the complexity of the fitting procedure with several dozen free parameters, the DE algorithm was used. All of the classical strategies and their tuning parameters were tested, and the best DE strategy for fitting of monomeric pigments had been found.

PSIIRC is a system of interacting pigments fixed in the protein skeleton and, in comparison with monomers, needs additional computational procedures such as matrix diagonalization (eigenstate problem) and integrations over a time scale to assess the relaxation rates. As in the case of monomers, we perform the strategy tests for PSIIRC modeling. The test results showed that the *DE/rand-to-best/1/exp* and *DE/best/1/bin* strategies are the best choices for the system; however, after thoroughly testing the strategy parameters $\{F, Cr\}$, it was found that each of those two has its own advantages and disadvantages.

For such computational algorithms, sticking at local minima for high-dimensional multimodal function is a rather serious problem. The global solution to this problem will sufficiently simplify the calculations because when the algorithm passes through the last local minimum, the rate of convergence becomes clearly exponential (Figure 5). In fact, with an increase in the number of free parameters, the convergence probability decreases greatly. Even with optimal values of the parameters, the percentage of convergence has a certain limit, which is determined by the initial conditions and the statement of a specific problem.

For example, with the best tuning parameters $\{F = 0.55, Cr = 0.9\}$, the convergence rate for the *DE/rand-to-best/1/exp* strategy with nine unknown parameters is equal about 27%. *DE/best/1/bin* cannot find the best solution and is always stuck. It is worth noting that with an increase in the number of unknowns, the value of the best tuning parameters is retained. Therefore, the next step in solving the problem will be the creation (development) of the algorithm, which can determine local minimum and after it can get out of there. A more flexible selection of tuning parameters [27,28,41] (for example, an adaptation of the SADE algorithm [29,42]) or a way to get out from the local minima could make a wide step towards solving this problem.

8. Conclusions

We have shown that the use of a heuristic evolutionary algorithm such as DE in modeling the optical properties of PPCs allows us to obtain high-quality calculated spectra and, at the same time, to assess the uniqueness of the obtained parameters of the exciton model of the energy transfer in PPCs.

In this study, the DE algorithm was used for simulation of the linear optical response of a system of interacting chlorophyll and pheophytin pigments. Applying the MBOM and the theory of molecular excitons, we have demonstrated that the linear optical response of the PSIIRC (absorption, circular and linear dichroism, and steady-state fluorescence) can be fitted by DE with high accuracy. To explore the effectiveness of DE, we used the simulated experimental data as the target functions instead of those of actually measured. After the strategy test was performed, it appeared that only 2 of the 10 DE strategies have shown the best performance of the optimization algorithm. The best tuning parameters were determined to run the full optimization of PSIIRC linear optical response modeling. Finally, using the *DE/rand-to-best/1/exp* strategy, we found the exact solution for the PSIIRC exciton model and fitted the spectra with a reasonable convergence rate.

However, the chosen "optimal" strategies and their settings still do not allow us to find the desired exciton models of pigment–protein complexes with 100% probability. The main problem is that the optimization algorithm becomes stuck in the local minima (Figure 4 is a typical example). Thus, the development of modified DE strategies that can detect local minima and allow the algorithm to find ways to bypass them in the parameter space that minimizes the objective function is the immediate goal of our further research in this field.

Author Contributions: Validation, formal analysis, investigation, software, writing—original draft preparation, D.D.C.; conceptualization, methodology, resources, software, writing—original draft preparation, writing—review and editing, visualization, supervision, project administration, funding acquisition, R.Y.P. All authors have read and agreed to the published version of the manuscript.

Funding: This research was funded by a grant of the Ministry of Science and Higher Education of the Russian Federation for large scientific projects in priority areas of scientific and technological development (subsidy identifier 075-15-2020-774).

Institutional Review Board Statement: Not applicable.

Informed Consent Statement: Not applicable.

Data Availability Statement: No additional data available.

Acknowledgments: This study was carried out using equipment of the shared research facilities of the HPC computing resources at Moscow State University.

Conflicts of Interest: The authors declare no conflict of interest. The funders had no role in the design of the study, in the collection, analyses, or interpretation of the data, in the writing of the manuscript, or in the decision to publish the results.

References

1. Jang, S.J.; Mennucci, B. Delocalized excitons in natural light-harvesting complexes. *Rev. Mod. Phys.* **2018**, *90*, 035003. [CrossRef]
2. Mirkovic, T.; Ostroumov, E.E.; Anna, J.M.; van Grondelle, R.; Scholes, G.D. Light Absorption and Energy Transfer in the Antenna Complexes of Photosynthetic Organisms. *Chem. Rev.* **2017**, *117*, 249–293. [CrossRef] [PubMed]
3. Croce, R.; van Amerongen, H. Natural strategies for photosynthetic light harvesting. *Nat. Chem. Biol.* **2014**, *10*, 492–501. [CrossRef] [PubMed]
4. Pishchalnikov, R.Y.; Yaroshevich, I.A.; Slastnikova, T.A.; Ashikhmin, A.A.; Stepanov, A.V.; Slutskaya, E.A.; Friedrich, T.; Sluchanko, N.N.; Maksimov, E.G. Structural peculiarities of keto-carotenoids in water-soluble proteins revealed by simulation of linear absorption. *Phys. Chem. Chem. Phys.* **2019**, *21*, 25707–25719. [CrossRef]
5. Chaillet, M.L.; Lengauer, F.; Adolphs, J.; Muh, F.; Fokas, A.S.; Cole, D.J.; Chin, A.W.; Renger, T. Static Disorder in Excitation Energies of the Fenna-Matthews-Olson Protein: Structure-Based Theory Meets Experiment. *J. Phys. Chem. Lett.* **2020**, *11*, 10306–10314. [CrossRef]
6. Adolphs, J.; Renger, T. How proteins trigger excitation energy transfer in the FMO complex of green sulfur bacteria. *Biophys. J.* **2006**, *91*, 2778–2797. [CrossRef] [PubMed]

7. Higgins, J.S.; Lloyd, L.T.; Sohail, S.H.; Allodi, M.A.; Otto, J.P.; Saer, R.G.; Wood, R.E.; Massey, S.C.; Ting, P.C.; Blankenship, R.E.; et al. Photosynthesis tunes quantum-mechanical mixing of electronic and vibrational states to steer exciton energy transfer. *Proc. Natl. Acad. Sci. USA* **2021**, *118*, e2018240118. [CrossRef] [PubMed]
8. Croce, R.; van Amerongen, H. Light-harvesting in photosystem I. *Photosynth. Res.* **2013**, *116*, 153–166. [CrossRef] [PubMed]
9. Pishchalnikov, R.Y.; Shubin, V.V.; Razjivin, A.P. The role of vibronic modes in formation of red antenna states of cyanobacterial PSI. *Photosynth. Res.* **2020**, *146*, 75–86. [CrossRef] [PubMed]
10. Gunther, L.M.; Jendrny, M.; Bloemsma, E.A.; Tank, M.; Oostergetel, G.T.; Bryant, D.A.; Knoester, J.; Kohler, J. Structure of Light-Harvesting Aggregates in Individual Chlorosomes. *J. Phys. Chem. B* **2016**, *120*, 5367–5376. [CrossRef]
11. Ueno, S.; Tanimura, Y. Modeling and Simulating the Excited-State Dynamics of a System with Condensed Phases: A Machine Learning Approach. *J. Chem. Theory Comput.* **2021**, *17*, 3618–3628. [CrossRef] [PubMed]
12. Jansen, T.L.C. Computational spectroscopy of complex systems. *J. Chem. Phys.* **2021**, *155*, 170901. [CrossRef] [PubMed]
13. Mukamel, S. *Principles of Nonlinear Optical Spectroscopy*; Oxford University Press: New York, NY, USA; Oxford, UK, 1995; Volume 6, p. 543.
14. Kubo, R. Generalized Cumulant Expansion Method. *J. Phys. Soc. Jpn.* **1962**, *17*, 1100–1120. [CrossRef]
15. Lax, M. The Franck-Condon Principle and Its Application to Crystals. *J. Chem. Phys.* **1952**, *20*, 1752–1760. [CrossRef]
16. Abramavicius, D.; Palmieri, B.; Voronine, D.V.; Sanda, F.; Mukamel, S. Coherent Multidimensional Optical Spectroscopy of Excitons in Molecular Aggregates; Quasiparticle versus Supermolecule Perspectives. *Chem. Rev.* **2009**, *109*, 2350–2408. [CrossRef] [PubMed]
17. Brixner, T.; Hildner, R.; Kohler, J.; Lambert, C.; Wurthner, F. Exciton Transport in Molecular Aggregates—From Natural Antennas to Synthetic Chromophore Systems. *Adv. Energy Mater.* **2017**, *7*, 1700236. [CrossRef]
18. Holland, J.H. *Adaptation in Natural and Artificial Systems: An Introductory Analysis with Applications to Biology, Control, and Artificial Intelligence*; University of Michigan Press: Ann Arbor, MI, USA, 1975; p. 183.
19. Goldberg, D.E. *Genetic Algorithms in Search, Optimization and Machine Learning*, 13th ed.; Addison-Wesley Publishing Company, Inc.: Reading, MA, USA, 1989; p. 432.
20. Storn, R.; Price, K. Differential evolution—A simple and efficient heuristic for global optimization over continuous spaces. *J. Glob. Optim.* **1997**, *11*, 341–359. [CrossRef]
21. Storn, R. System design by constraint adaptation and differential evolution. *IEEE Trans. Evol. Comput.* **1999**, *3*, 22–34. [CrossRef]
22. Pishchalnikov, R.Y.; Bondarenko, A.A.; Ashikhmin, A.A. Optimizing the Multimode Brownian Oscillator Model for the Optical Response of Carotenoids in Solution by Fine Tuning of Differential Evolution. *Lobachevskii J. Math.* **2020**, *41*, 1545–1553. [CrossRef]
23. Pishchalnikov, R. Application of the differential evolution for simulation of the linear optical response of photosynthetic pigments. *J. Comput. Phys.* **2018**, *372*, 603–615. [CrossRef]
24. Das, S.; Mullick, S.S.; Suganthan, P.N. Recent advances in differential evolution—An updated survey. *Swarm Evol. Comput.* **2016**, *27*, 1–30. [CrossRef]
25. Rocca, P.; Oliveri, G.; Massa, A. Differential Evolution as Applied to Electromagnetics. *IEEE Antennas Propag. Mag.* **2011**, *53*, 38–49. [CrossRef]
26. Wu, G.H.; Mallipeddi, R.; Suganthan, P.N.; Wang, R.; Chen, H.K. Differential evolution with multi-population based ensemble of mutation strategies. *Inf. Sci.* **2016**, *329*, 329–345. [CrossRef]
27. Qin, A.K.; Huang, V.L.; Suganthan, P.N. Differential Evolution Algorithm with Strategy Adaptation for Global Numerical Optimization. *IEEE Trans. Evol. Comput.* **2009**, *13*, 398–417. [CrossRef]
28. Paterlini, S.; Krink, T. Differential evolution and particle swarm optimisation in partitional clustering. *Comput. Stat. Data Anal.* **2006**, *50*, 1220–1247. [CrossRef]
29. Liu, J.; Lampinen, J. A fuzzy adaptive differential evolution algorithm. *Soft Comput.* **2005**, *9*, 448–462. [CrossRef]
30. Gelzinis, A.; Abramavicius, D.; Ogilvie, J.P.; Valkunas, L. Spectroscopic properties of photosystem II reaction center revisited. *J. Chem. Phys.* **2017**, *147*, 115102. [CrossRef] [PubMed]
31. Raszewski, G.; Saenger, W.; Renger, T. Theory of optical spectra of photosystem II reaction centers: Location of the triplet state and the identity of the primary electron donor. *Biophys. J.* **2005**, *88*, 986–998. [CrossRef] [PubMed]
32. Novoderezhkin, V.I.; Andrizhiyevskaya, E.G.; Dekker, J.P.; van Grondelle, R. Pathways and timescales of primary charge separation in the photosystem II reaction center as revealed by a simultaneous fit of time-resolved fluorescence and transient absorption. *Biophys. J.* **2005**, *89*, 1464–1481. [CrossRef]
33. Muh, F.; Plockinger, M.; Renger, T. Electrostatic Asymmetry in the Reaction Center of Photosystem II. *J. Phys. Chem. Lett.* **2017**, *8*, 850–858. [CrossRef] [PubMed]
34. Renger, G.; Renger, T. Photosystem II: The machinery of photosynthetic water splitting. *Photosynth. Res.* **2008**, *98*, 53–80. [CrossRef]
35. Renger, T. Semiclassical Modified Redfield and Generalized Forster Theories of Exciton Relaxation/Transfer in Light-Harvesting Complexes: The Quest for the Principle of Detailed Balance. *J. Phys. Chem. B* **2021**, *125*, 6406–6416. [CrossRef] [PubMed]
36. Pishchalnikov, R.Y.; Shubin, V.V.; Razjivin, A.P. Spectral differences between monomers and trimers of photosystem I depend on the interaction between peripheral chlorophylls of neighboring monomers in trimer. *Phys. Wave Phenom.* **2017**, *25*, 185–195. [CrossRef]

37. Trinkunas, G.; Holzwarth, A.R. Kinetic modeling of exciton migration in photosynthetic systems. 3. Application of genetic algorithms to simulations of excitation dynamics in three-dimensional photosystem core antenna reaction center complexes. *Biophys. J.* **1996**, *71*, 351–364. [CrossRef]
38. Trinkunas, G.; Connelly, J.P.; Muller, M.G.; Valkunas, L.; Holzwarth, A.R. Model for the excitation dynamics in the light-harvesting complex II from higher plants. *J. Phys. Chem. B* **1997**, *101*, 7313–7320. [CrossRef]
39. Vaitekonis, S.; Trinkunas, G.; Valkunas, L. Red chlorophylls in the exciton model of photosystem I. *Photosynth. Res.* **2005**, *86*, 185–201. [CrossRef] [PubMed]
40. Bruggemann, B.; Sznee, K.; Novoderezhkin, V.; van Grondelle, R.; May, V. From structure to dynamics: Modeling exciton dynamics in the photosynthetic antenna PS1. *J. Phys. Chem. B* **2004**, *108*, 13536–13546. [CrossRef]
41. Gong, W.Y.; Cai, Z.H. Differential Evolution With Ranking-Based Mutation Operators. *IEEE Trans. Cybern.* **2013**, *43*, 2066–2081. [CrossRef] [PubMed]
42. Noman, N.; Iba, H. Accelerating differential evolution using an adaptive local search. *IEEE Trans. Evol. Comput.* **2008**, *12*, 107–125. [CrossRef]